2024 IEEE/ASME International Conference on Advanced Intelligent Mechatronics (AIM)
July 15-19, 2024. Boston, MA, USA

Development and Evaluation of an Experimental Platform for State-of-Charge Balancing Control of Lithium-Ion Battery Systems

Jiaao Wang[1], M. Chase Carson[1], Yangyang Qian[1], Zongli Lin[1], and Yacov A. Shamash[2]

***Abstract*— Numerous battery management system (BMS) algorithms aimed at achieving state-of-charge (SOC) balancing have been proposed. This paper reports on the development and evaluation of an experimental platform for testing BMS algorithms. The platform we developed allows for simple parameter or physical quantity expression tweaks, making it easier to assess the performances of different various BMS algorithms. The hardware of the platform comprises a DSP chip (TMS320F28335), a custom-designed buck converter, various battery packs, and load resistors. By simulating circuit operations and analyzing battery output under load, an SOC versus open-circuit voltage graph is produced for estimation of the SOC. Employing cascaded PI controllers for the buck converter, the platform demonstrates its capability in power control and battery balance management through tests on a single battery system and on multiple battery systems. A BMS algorithm is selected for platform evaluation, affirming its effectiveness in maintaining SOC balancing among heterogeneous battery units.**

***Index Terms*— Battery systems, experimental platform, SOC estimation, SOC balancing.**

I. Introduction

Battery energy storage systems (BESSs) play a critical role in enhancing the integration of renewable energy sources, such as solar and wind power, into smart grids. By storing excess energy generated during peak production times and releasing it during periods of high demand or low production, BESSs help in balancing supply and demand, thus increasing the reliability and stability of the power grid [1, 2]. Among these battery systems, lithium-ion battery systems are preferred [3] due to their high energy density, long lifespan, high voltage capacity, and low self-discharge rate, which make them ideal for portable electronics, electric vehicles, and grid storage [4–6]. Battery management systems (BMSs) are crucial for managing and protecting battery packs, particularly in applications involving lithium-ion batteries.

The state of charge (SOC) within a battery is a fundamental metric [7] that signifies the current charge level of a battery with respect to its maximum capacity. This metric is indicative of the available energy within the battery [8], facilitating efficient energy management [9]. It is important to monitor SOC levels [10], enabling the BMS to pinpoint batteries in need of maintenance or substitution [11]. Thus, various methods exist for SOC estimation, for example, the table lookup method [12]. SOC balancing is crucial for battery systems as it equalizes SOC levels across all battery units [13], maximizing capacity, prolonging lifespan, enhancing safety, and improving efficiency. It prevents overcharging and deep discharging of individual battery units, reducing the risk of overheating and damage [14]. In [15], an SOC balancing control algorithm requiring global information is presented for BESSs. To relax the requirement of global information, a distributed cooperative control algorithm is proposed in [16] for SOC balancing of BESSs.

Numerous studies have demonstrated promising simulation outcomes and experimentally validated the feasibility of SOC balancing control algorithms. In this study, our objective is to develop a general experimental platform for battery systems, for example, lithium-ion battery systems. This platform is designed to facilitate the testing and validation of advanced SOC balancing control algorithms that have been recently proposed for BESSs, such as those in [15, 16]. A schematic diagram of our experimental platform is shown in Fig. 1, where each battery system is composed of a battery unit and a power converter. Each battery unit outputs power through a programmable buck converter, and a DSP chip is utilized to regulate the output voltage, current, or power of the battery. Within the platform, the electrical equivalent circuit model in [17], alongside an external load resistor, is used to represent circuit operations. This representation enables the estimation of the SOC of each battery unit, modeled as a relationship with the open-circuit voltage [18].

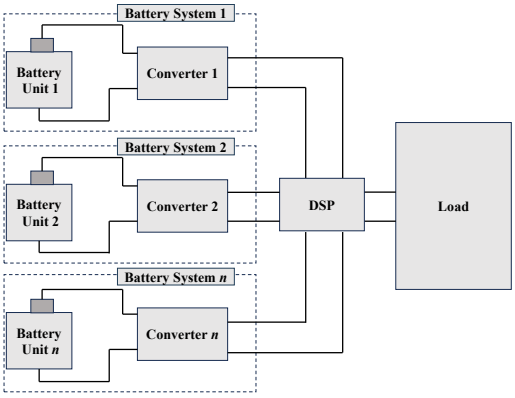

Fig. 1. Schematic diagram of the experimental platform.

To evaluate the developed platform, we first conduct

This work relates to Department of Navy awards N00014-22-1-2001 and N00014-23-1-2124 issued by the Office of Naval Research. The United States Government has a royalty-free license throughout the world in all copyrightable material contained herein. *(Corresponding author: Zongli Lin.)*

[1]Jiaao Wang, M. Chase Carson, Yangyang Qian, and Zongli Lin are with the Charles L. Brown Department of Electrical and Computer Engineering, University of Virginia, Charlottesville, VA 22904 USA. rdj7eq@virginia.edu; mcc5xb@virginia.edu; jbt4up@virginia.edu; zl5y@virginia.edu

[2]Yacov A. Shamash is with the Department of Electrical and Computer Engineering, Stony Brook University, Stony Brook, NY 11794 USA. yacov.shamash@stonybrook.edu

performance evaluation for a single battery system. For local converter control within the battery system, we adopt cascaded voltage and current control loops, using proportional-integral (PI) controllers. Experimental results show that the battery's output voltage can be quickly regulated to a voltage set-point and so is the battery's output power. We next conduct performance evaluation for multiple battery systems. In experiments, we implement the SOC balancing control algorithm proposed in [15] on the platform composed of four heterogeneous battery units. Experimental results validate the SOC balancing capacity on the developed platform.

The remainder of this paper is outlined as follows. Section II describes the development of our experimental platform, including the platform architecture, converter control, data collection, and SOC estimation. Subsequently, experimental tests are conducted in Section III to evaluate the performance of the developed experimental platform. Specifically, experimental results are presented for voltage control of single battery systems and for SOC balancing control of multiple battery systems. Finally, Section IV concludes this paper.

II. Development of the Platform

In this section, we present the development of an experimental platform for lithium-ion battery systems, as shown in Fig. 1.

A. Platform Architecture

The platform is centered around a DSP chip TMS320F28335, selected for its precision in controlling the EPWM output target values and its signal processing capabilities that facilitate the realization of complex control algorithms. The prototype of the developed experimental platform is depicted in Fig. 2.

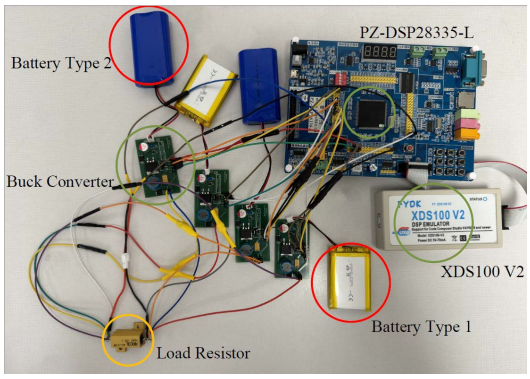

Fig. 2. Prototype of the experimental platform.

As for the hardware foundation, the PZ-DSP28335-L development board is chosen, incorporating the TMS320F28335 chip, and equipped with multiple ADC interfaces for real-time voltage monitoring required by the control algorithm. Additionally, the development board is equipped with an RS232 module to facilitate data transmission to a host computer. The emulator used in our platform is the XDS 100V2, which allows for comprehensive testing and debugging. The load is chosen as a constant resistor with a resistance of 1.6Ohms, ensuring a stable environment for testing the BMS under consistent load conditions. The experimental setup employs two distinct types of battery packs, 974058 rechargeable lithium-ion polymer batteries (Battery Type 1, 3.7V, 3000mAh) and 18650 rechargeable lithium-ion batteries (Battery Type 2, 3.7V, 4400mAh). Each battery pack is connected to a buck converter. The buck converters are chosen to be the same across the battery packs.

To control a battery system, a DC-DC buck converter is constructed to regulate the output voltage of the battery. The components of the buck converter we designed are listed in Table 1. This buck converter, a form of non-isolated DC-DC switching converter, efficiently converts a higher input voltage to a lower output voltage. The basic topology of the buck converter is depicted in Fig. 3.

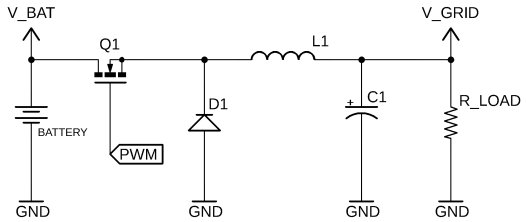

Fig. 3. Topology of the buck converter.

To accommodate parallel operations of several buck converters, we need to enhance the buck converter in Fig. 3. A schematic of the enhanced buck converter is shown in Fig. 4. Enhancements include the addition of a diode (D2) for current OR-ing, a gate driver (U1) for efficient MOSFET operations and a current-sensing resistor (R1) for supply current measurement. Additional features, such as a battery connector (JP2), test points (JP4, JP5), and swappable load resistance (JP6), are integrated to facilitate testing and versatility. Additionally, an input capacitor (C2) and an external microcontroller connection header (JP3) are incorporated to improve stability and control. Fig. 5 shows the PCB post-fabrication of the enhanced buck converter.

B. Converter Control

A schematic of the local control for a buck converter within a battery system is shown in Fig. 6, where two cascaded PI controllers are used to regulate the converter's output voltage and current.

To illustrate the control process, we take the buck converter associated with battery 1 as an example. For the voltage controller (PI controller), we set the input signal as the error between the reference voltage, termed Target Voltage 1, and the measured output voltage of converter 1. This reference voltage is related to the power set-point determined by the power control algorithm for SOC balancing. The output signal of the voltage controller, termed PI Output 1, is then sent to the current controller, as the reference current. For the current controller (PI controller), the input signal is set as the error between the reference current and the measured output current of converter 1. Finally, the output signal of the current controller, termed PI Output 2, is used to

TABLE I

COMPONENT SPECIFICATIONS

Name	Manufacturer Product Number	Important parameters
D1, D2	GSGC1545SA	Rectifier, Schottky, 15A, 45V, E
Q1	IRLZ44SPBF	N-Channel 60V 50A (Tc) 3.7W (Ta), 150W (Tc)
L1	SBC6-4R7-802	4.7µH Unshielded Drum Core, Wirewound Inductor 8A 10mOhm Max Radial
C1	TPSD477M006R0100	470µF Molded Tantalum Capacitors 6.3V 2917 (7343 Metric) 100mOhm
C2	RL80J102MDN1KX	1000µF 6.3V Aluminum - Polymer Capacitors Radial
C3	FK16X7R1C106KR020	10µF ±10% 16V Ceramic Capacitor X7R Radial
R1	WSL2010R1000FEA18	100mOhms ±1% 1W Chip Resistor 2010 (5025 Metric)

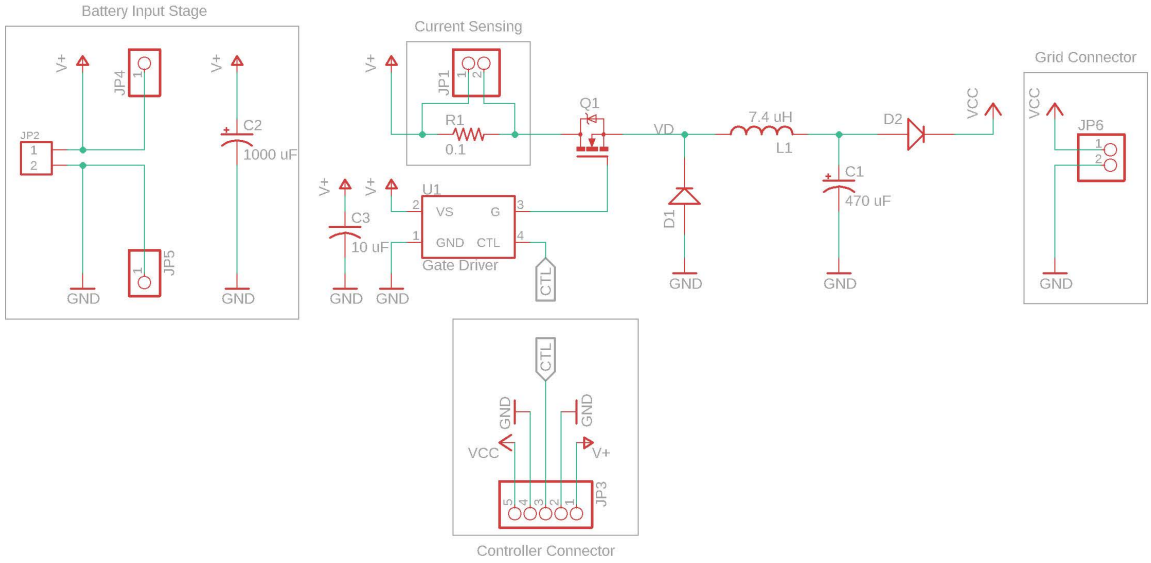

Fig. 4. Schematic of the enhanced buck converter.

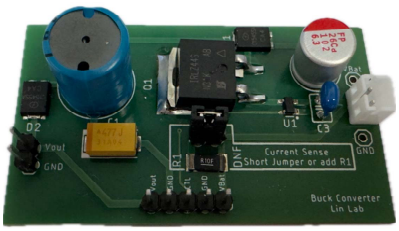

Fig. 5. Prototype of the enhanced buck converter.

generate a PWM signal, as a control signal, for the switch of converter 1. Through the above two cascaded PI controllers, the output power of converter 1 can quickly track the desired power set-point.

The power set-point for the converter's output power is determined by SOC balancing control algorithms. In this study, we will implement the control algorithm in [15], stated as follows. For each battery unit i, we define

$$\tau_i = SOC_i \times Q_i \times V_{\text{in}i}, \tag{1}$$

where SOC_i is the SOC, Q_i is the battery's capacity, and $V_{\text{in}i}$ is the battery's voltage, which is the input voltage to buck converter i. Then, the power set-point of buck converter i is

$$P_{\text{ref}i} = \left(\frac{\tau_i}{\tau_{\text{avg}}}\right) \times \frac{P_{\text{load}}}{N}, \tag{2}$$

where $\tau_{\text{avg}} = \frac{1}{N}\sum_{i=1}^{N} \tau_i$, N is the number of battery units, and P_{load} is the load power.

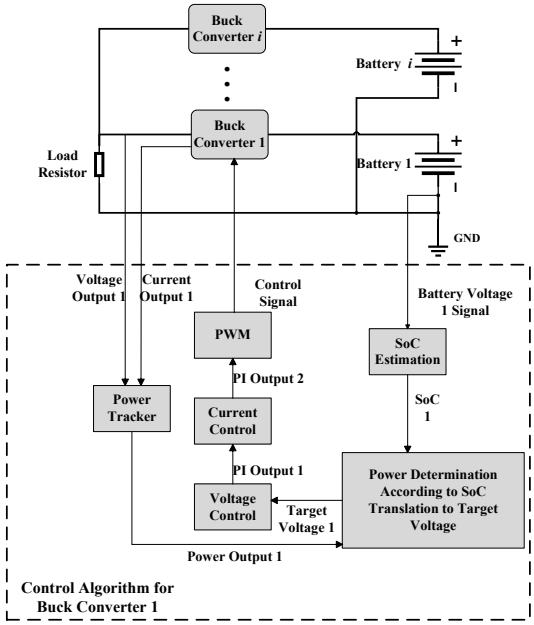

Fig. 6. Schematic of the local control for a buck converter.

C. Data Collection

Given that the development board PZ-DSP28335-L is equipped with multiple ADC (Analog-to-Digital Converter) jumpers, it is feasible to sequentially measure the voltage values at these jumpers. Consequently, we leverage the ADC-

converted digital values to determine the voltage value at the interface, according to the equation,

$$\text{Voltage Value} = \frac{3 \times \text{ADC Data Value}}{4096}. \tag{3}$$

In the case of a single battery supply, the output power is directly calculable from the obtained output voltage. In the presence of a constant resistive load, the relationship between the output power P_{output} and the load power P_{load} is

$$P_{\text{load}} = \frac{V_{\text{out}}^2}{R_{\text{load}}}. \tag{4}$$

Because the load is a constant resistor, the output current is calculated based on the buck converter's output as

$$I_{\text{out}} = \frac{V_{\text{out}}}{R_{\text{load}}}. \tag{5}$$

Additionally, the output power of the battery is given by

$$P_{\text{out}} = V_{\text{out}} \times I_{\text{load}} = \frac{V_{\text{out}}^2}{R_{\text{load}}}. \tag{6}$$

However, in the case when multiple battery units are connected in parallel, it is not feasible to calculate the branch circuit current using the same way as in the case of a single battery unit. To address this issue, we add a measuring resistor in each branch after the buck converter, as shown in Fig. 7, to assist in measuring the current in the branch. Specifically, we set the resistance of the measuring resistor as $R_{\text{MeasureResistor}} = 0.3\Omega$. Then, by measuring the output voltage V_{out1} of converter 1, we calculate the voltage drop across measuring resistor 1 as

$$V_{\text{MeasureResistor1}} = V_{\text{load}} - V_{\text{out1}}, \tag{7}$$

where V_{load} is the measured voltage across the load. The output current of buck converter 1 on the branch is equal to the current through measure resistor 1, given by

$$I_{\text{out1}} = \frac{V_{\text{measure1}}}{R_{\text{MeasureResistor}}}. \tag{8}$$

Furthermore, the output power of buck converter 1 is

$$P_{\text{out1}} = V_{\text{out1}} \times I_{\text{out1}}. \tag{9}$$

The output power P_{out1} in (9) is used as the measured output power of buck converter 1. The control objective is to make the measured output power P_{out1} track the power set-point $P_{\text{ref}i}$ given by (2).

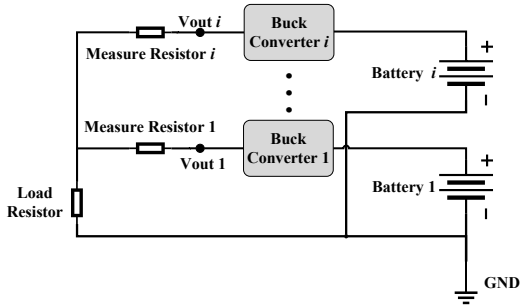

Fig. 7. Schematic of multiple battery units in parallel.

D. SOC Estimation

We adopt the look-up table method for estimating the SOC of the battery, involving real-time voltage readings during battery operations. A pre-established table correlating SOC values to battery voltage facilitates immediate SOC determination upon acquiring the battery's voltage. In the following, we provide an in-depth explanation of the process involved in constructing the SOC-voltage relationship table.

The internal resistance, or Equivalent Series Resistance (ESR), is a pivotal parameter of a battery influencing its performance and efficiency. We delineate a method for the ESR quantification, starting with the open-circuit voltage (OCV) measurement of the battery. The procedure starts with the OCV measurement, denoted as U_0, followed by a succinct short-circuiting of the battery terminals to establish a baseline voltage. Thereafter, a resistor, R_0, is connected in parallel to the battery terminals to trigger a discharge cycle. During this discharge phase, the voltage across the battery terminals, U, is recorded. Then, the ESR can be computed utilizing the following equation,

$$ESR = \frac{U_0 - U}{U/R_0}. \tag{10}$$

By applying the above method to two types of distinct lithium-ion batteries, we have the following outcomes: For Battery Type 1 (3000mAh, 3.7V), the calculated ESR is 0.142Ohm; For Battery Type 2 (4400mAh, 3.7V), the calculated ESR is 0.202Ohm.

Fig. 8 illustrates the circuit configuration employed for measuring the relationship between the battery's voltage and SOC. An external load resistor, characterized by a resistance R_{load}, is connected to the battery. The battery discharges continuously from a fully charged state, maintaining a constant discharge rate.

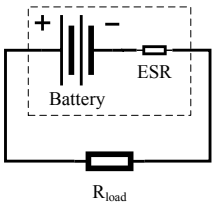

Fig. 8. Schematic of the measurement circuit.

Let I_{closed} represent the operating current of the circuit and V_{load} denote the voltage across the load resistor. Then, I_{closed} is calculated as

$$I_{\text{closed}} = \frac{V_{\text{load}}}{R_{\text{load}}}. \tag{11}$$

The voltage drop across the battery's internal resistance V_{ESR} is given by

$$V_{\text{ESR}} = I_{\text{closed}} \times \text{ESR}. \tag{12}$$

Consequently, the open-circuit voltage $V_{\text{open\_circuit}}$ can be expressed as

$$V_{\text{open\_circuit}} = V_{\text{load}} + V_{\text{ESR}}. \tag{13}$$

Taking Battery Type 1 (3000mAh, 3.7V) as an example, the relationship between the open-circuit voltage and the operating voltage under load conditions is shown in Fig. 9.

The power consumed by the load P_{load} is calculated as

$$P_{\text{load}} = \frac{V_{\text{load}}^2}{R_{\text{load}}}. \tag{14}$$

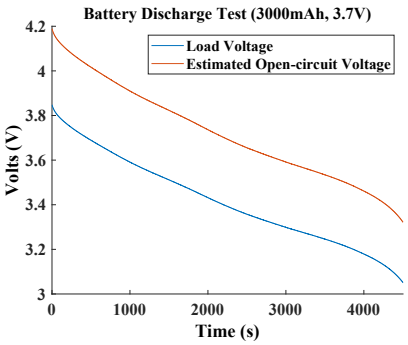

Fig. 9. Relationship between open-circuit and operating voltage .

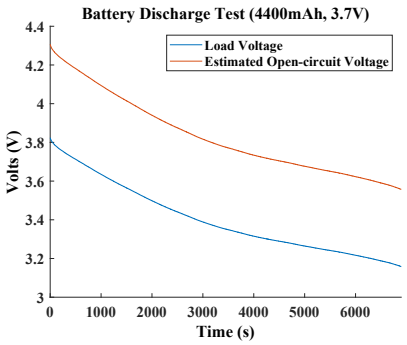

Fig. 11. Relationship between open-circuit and operating voltage.

The total energy expended by the battery throughout the discharge process, E_{consumed}, is obtained through the integration of P_{load} over time as

$$E_{\text{consumed}} = \int P_{\text{load}}\, \mathrm{d}t. \tag{15}$$

The consumed charge C_{consumed} is derived from (15) as

$$C_{\text{consumed}} = \frac{E_{\text{consumed}}}{V_{\text{load}} \times 3.6}. \tag{16}$$

By combining the consumed charge C_{consumed} with the initial charge C_0, the SOC can be determined by

$$\text{SOC} = \left(\frac{C_0 - C_{\text{consumed}}}{C_0} \right) \times 100\%. \tag{17}$$

Consequently, in conjunction with the voltage-time relationship shown in Fig. 9, a plot of SOC versus voltage is obtained, as shown in Fig. 10. The plot in Fig. 10 is usually called a look-up table, which enables the determination of the battery's SOC during the circuit experiment by measuring the battery's voltage.

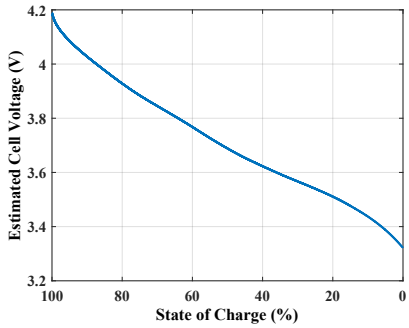

Fig. 10. SOC (3000mAh) versus open-circuit voltage.

Similarly, for Battery Type 2 (4400mAh, 3.7V), we can obtain the relationship between open-circuit and operating voltage and the look-up table between SOC and open-circuit voltage, which are shown in Figs. 11 and 12, respectively.

III. Evaluation of the Platform

A. Performance Evaluation for Single Battery Systems

We first conduct performance evaluation for an individual battery system. In the experimental test, we need to select appropriate parameters for two PI controllers. A set of gains

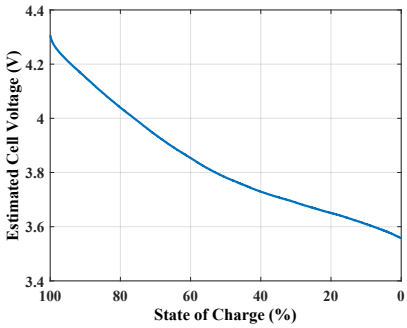

Fig. 12. SOC (4400mAh) versus open-circuit voltage.

are selected to tailor to the system's response characteristics. Specifically, the first PI controller is configured with the gains $P = 12$ and $I = 1$. Following the initial voltage adjustment, the second PI controller receives the processed signal for further refinement. The gains for the second PI controller are chosen as $P_1 = 0.1$ and $I_1 = 0.05$.

To evaluate the performance of the designed battery control system, we consider a step response test. The experimental setup includes the connection of a solitary battery pack, with the load of a solid-state resistor. In the test, a discrete step function is applied to specify the voltage setpoint of an individual battery system. This function is defined by

$$V_{\text{ref}}(t) = \begin{cases} 0.5V & \text{if } 40l \le t < 40l + 10, \\ 1.0V & \text{if } 40l + 10 \le t < 40l + 20, \\ 1.5V & \text{if } 40l + 20 \le t < 40l + 30, \\ 2.0V & \text{if } 40l + 30 \le t < 40(l + 1), \end{cases} \tag{18}$$

where l is a non-negative integer.

The response of the battery system to the voltage set-point given by (18) is depicted in Fig. 13. As seen in Fig. 13, the output voltage of the buck converter quickly tracks the step changes in the voltage setpoint. This illustrates the efficacy of PI controllers in maintaining the desired voltage levels. The system's performance in this experiment substantiates its potential applicability in real-world scenarios, where precise voltage control is imperative.

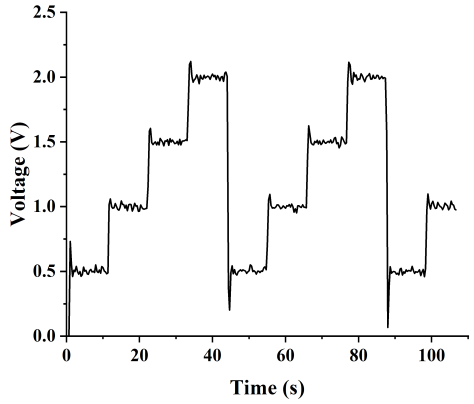

Fig. 13. Experiment result for voltage regulation of a single battery system.

B. Performance Evaluation for Multiple Battery Systems

We now conduct performance evaluation for multiple battery systems. In this experimental test, we use the same PI parameter setting as that in the case of a single battery system and set the load power as $P_{\text{load}} = 4.5W$. Then, we test the SOC balancing among four battery units. Among them, two battery units belongs to Battery Type 1 and the other two battery units belong to Battery Type 2.

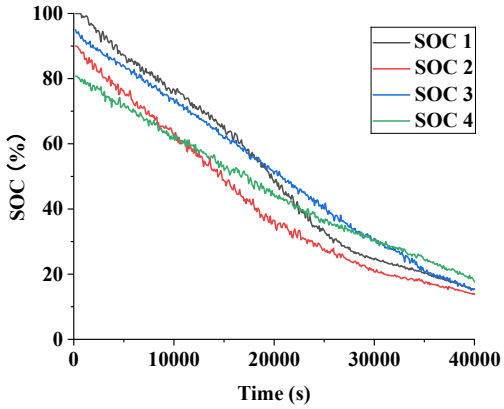

Fig. 14. Experimental result for SOC balancing among four battery systems.

Fig. 14 presents the result of the experimental test conducted to assess the SOC balancing capabilities by applying the control algorithm (2). In Fig. 14, SOC 1 and SOC 2 are for Type 1 batteries, and SOC 3 and SOC 4 are for Type 2 batteries. It can be observed that the SOC levels converge towards the same value but with some fluctuations. This is because of inaccuracy in the measurement of the voltage values.

IV. Conclusions

We developed an experimental platform for testing BMS algorithms for batteries. The platform consists of a DSP chip (TMS320F28335), a custom-designed buck converter, battery packs, and load resistors. Moreover, we evaluated the platform's performance through tests involving both single battery systems and multiple battery systems. Particularly, we validated the efficacy of an existing control algorithm in maintaining SOC balancing among heterogeneous battery units. Future work may include: 1) implementing distributed SOC balancing control algorithms for more complex testing scenarios, 2) refining the buck converter's structure to simplify the measurement of voltage and current directly from the battery, and 3) enhancing the measurement accuracy to ensure more precise SOC estimation.

References

[1] B. M. Gundogdu, S. Nejad, D. T. Gladwin, M. P. Foster, and D. A. Stone, "A battery energy management strategy for UK enhanced frequency response and triad avoidance," *IEEE Transactions on Industrial Electronics*, vol. 65, no. 12, pp. 9509–9517, 2018.

[2] H. Chen, T. N. Cong, W. Yang, C. Tan, Y. Li, and Y. Ding, "Progress in electrical energy storage system: A critical review," *Progress in Natural Science*, vol. 19, no. 3, pp. 291–312, 2009.

[3] I. B. Espedal, A. Jinasena, O. S. Burheim, and J. J. Lamb, "Current trends for state-of-charge (SoC) estimation in lithium-ion battery electric vehicles," *Energies*, vol. 14, no. 11, p. 3284, 2021.

[4] X. Feng, M. Ouyang, X. Liu, L. Lu, Y. Xia, and X. He, "Thermal runaway mechanism of lithium ion battery for electric vehicles: A review," *Energy Storage Materials*, vol. 10, pp. 246–267, 2018.

[5] L. J. Aaldering, J. Leker, and C. H. Song, "Analysis of technological knowledge stock and prediction of its future development potential: The case of lithium-ion batteries," *Journal of Cleaner Production*, vol. 223, pp. 301–311, 2019.

[6] B. Diouf and R. Pode, "Potential of lithium-ion batteries in renewable energy," *Renewable Energy*, vol. 76, pp. 375–380, 2015.

[7] H. Rahimi-Eichi, U. Ojha, F. Baronti, and M.-Y. Chow, "Battery management system: An overview of its application in the smart grid and electric vehicles," *IEEE Industrial Electronics Magazine*, vol. 7, no. 2, pp. 4–16, 2013.

[8] D. Andrea, *Battery management systems for large lithium-ion battery packs*. Norwood, MA, USA: Artech House, 2010.

[9] Y. Wang, Z. Chen, and C. Zhang, "On-line remaining energy prediction: A case study in embedded battery management system," *Applied Energy*, vol. 194, pp. 688–695, 2017.

[10] X. Hu, D. Cao, and B. Egardt, "Condition monitoring in advanced battery management systems: Moving horizon estimation using a reduced electrochemical model," *IEEE/ASME Transactions on Mechatronics*, vol. 23, no. 1, pp. 167–178, 2018.

[11] N. A. Chaturvedi, R. Klein, J. Christensen, J. Ahmed, and A. Kojic, "Algorithms for advanced battery-management systems," *IEEE Control Systems Magazine*, vol. 30, no. 3, pp. 49–68, 2010.

[12] D. N. How, M. Hannan, M. H. Lipu, and P. J. Ker, "State of charge estimation for lithium-ion batteries using model-based and data-driven methods: A review," *IEEE Access*, vol. 7, pp. 136 116–136 136, 2019.

[13] K.-M. Lee, S.-W. Lee, Y.-G. Choi, and B. Kang, "Active balancing of li-ion battery cells using transformer as energy carrier," *IEEE Transactions on Industrial Electronics*, vol. 64, no. 2, pp. 1251–1257, 2017.

[14] J. Kim, J. Shin, C. Chun, and B. Cho, "Stable configuration of a li-ion series battery pack based on a screening process for improved voltage/SOC balancing," *IEEE Transactions on Power Electronics*, vol. 27, no. 1, pp. 411–424, 2012.

[15] L. Xing, Y. Mishra, Y.-C. Tian, G. Ledwich, C. Zhou, W. Du, and F. Qian, "Distributed state-of-charge balance control with event-triggered signal transmissions for multiple energy storage systems in smart grid," *IEEE Transactions on Systems, Man, and Cybernetics: Systems*, vol. 49, no. 8, pp. 1601–1611, 2019.

[16] T. Meng, Z. Lin, and Y. A. Shamash, "Distributed cooperative control of battery energy storage systems in DC microgrids," *IEEE/CAA Journal of Automatica Sinica*, vol. 8, no. 3, pp. 606–616, 2021.

[17] V. Johnson, "Battery performance models in ADVISOR," *Journal of Power Sources*, vol. 110, no. 2, pp. 321–329, 2002.

[18] M. Verbrugge and E. Tate, "Adaptive state of charge algorithm for nickel metal hydride batteries including hysteresis phenomena," *Journal of Power Sources*, vol. 126, no. 1-2, pp. 236–249, 2004.